Università degli studi di Udine

Versatile experimental setup for FTJ characterization

(Article begins on next page)

01 September 2024

Versatile experimental setup for FTJ characterization

M. Massarotto[a,*], F. Driussi[a], A. Affanni[a], S. Lancaster[b], S. Slesazeck[b], T. Mikolajick[b,c], D. Esseni[a]

[a]*DPIA, University of Udine, Via delle Scienze 206, 33100 Udine, Italy*
[b]*NaMLab gGmbH, Nöthnitzer Str. 64a, 01187 Dresden, Germany*
[c]*IHM TU Dresden, Nöthnitzer Str. 64, 01187 Dresden, Germany*

Abstract

Ferroelectric Tunnel Junctions (FTJ) are intriguing electron devices which can be operated as memristors and artificial synapses for hardware neural networks. In this work, two virtual–grounded amplifiers have been designed to characterize the hysteretic I–V and Q–V characteristics directly, and good agreement between repeated measurements on both circuits demonstrates the dependability and flexibility of the two setups. Optimal measurement conditions have also been assessed and, finally, wake–up, fatigue, and the preset–dependent early breakdown have been studied.

Keywords: Ferroelectric, Hafnium Oxide, Ferroelectric Tunnel Junction, Experimental Characterization, Endurance

1. Introduction

Ferroelectric HfO_2 offers a viable option for nonvolatile memory elements [1], also raising great interest as artificial synapses for hybrid memristive–CMOS circuits for spike–based neuromorphic computing [2, 3]. In this respect, Fer-

---

*Corresponding author
Email address: `massarotto.marco001@spes.uniud.it` (M. Massarotto)

roelectric Tunnel Junctions (FTJs) in a Metal–Ferroelectric–Dielectric–Metal structure (Fig. 1) are promising candidates as high impedance and low energy synaptic devices with multiple level operation [4].

FTJ optimization requires in–depth characterization, because of the delicate interplay between polarization stability, charge trapping and the read current [5, 6]. Hence, versatile measurement setups are needed to grasp the FTJ operation under different conditions. Here we propose an experimental setup able to characterize the FTJs going from the quasi–static regime, namely large–signals at low frequency, up to the small–signal analysis, typically performed at medium/high frequency. Specific design choices allowed us to measure either the current versus voltage (I–V) curves or directly the switching charge versus voltage (Q–V) characteristics. After its validation, the setup has been used to measure FTJs at different frequencies and cycling levels.

2. Device fabrication

FTJ devices were fabricated by depositing $10\,\text{nm}$ $\text{Hf}_{0.5}\text{Zr}_{0.5}\text{O}_2$ (HZO) and $2\,\text{nm}$ Al_2O_3 via atomic layer deposition (ALD) on bottom W $(30\,\text{nm})$/TiN $(10\,\text{nm})$ electrodes. $10\,\text{nm}$ TiN was deposited on top via reactive sputtering under ultra–high vacuum, for crystallization of the HZO layer as well as to form a top contact. The crystallization anneal was performed at $500\,°\text{C}$ for $20\,\text{s}$. Finally, capacitors were formed by depositing $10\,\text{nm}$ Ti/$25\,\text{nm}$ Pt through a shadow mask, used as a hardmask for SC–1 etching of the TiN layer.

3. Design of the experimental setup

To characterize the two–terminal FTJs, the simple, low–cost and versatile experimental setup sketched in Fig. 1 has been designed. An arbitrary waveform generator (*AG33250A*) is connected to the MF metal electrode of the FTJ under test, while the MD metal contact is instead connected to a virtual–grounded amplifier consisting of an OPAMP (*TL082CP*) and a feedback R—C pair (Fig. 1).
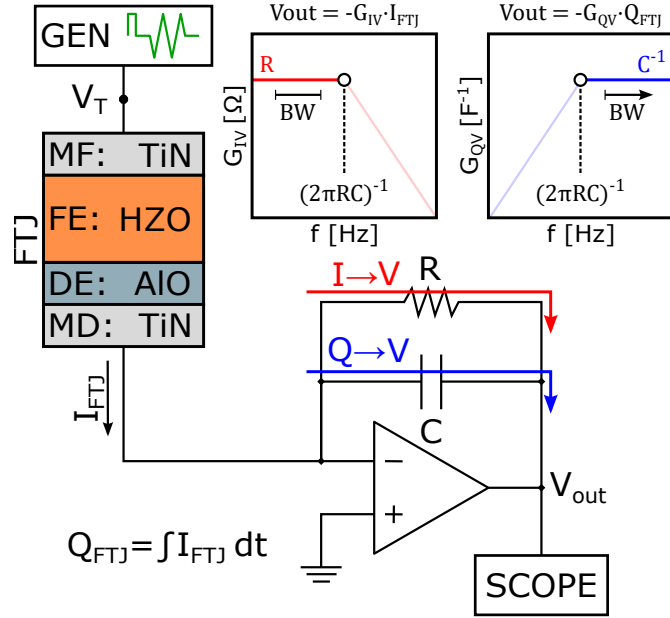
2

Figure 1: Experimental setup used to characterize the FTJs. The feedback amplifier can be used either as an I→V converter (R=1.5 kΩ, C=470 pF) or as a Q→V integrator (R=4.7 MΩ, C=3.9 nF) to directly measure I_{FTJ} or Q_{FTJ} respectively. Triangular pulses (V_T) are applied and V_{out} is monitored in time through an oscilloscope. The insets show the bandwidth (BW) of the circuits.

The current I_{FTJ} flows through the OPAMP feedback loop resulting in an output voltage V_{out} that is monitored through an oscilloscope (*TDS520B*). In this respect, depending on the R–C design, a current–to–voltage I→V converter or a charge–to–voltage Q→V integrator is realized. Both circuits share the same electrical scheme; however, for a given frequency f of the input signal, if $f \ll f_p = (2\pi RC)^{-1}$, the device current I_{FTJ} mainly flows on R, thus inducing $V_{out} \simeq R \cdot I_{FTJ}$ and effectively leading to an I→V converter, where the capacitor is simply used to attain an adequate stability margin for the feedback circuit. If $f \gg f_p$, instead, I_{FTJ} is integrated by the capacitor, thus resulting in $V_{out} \simeq Q_{FTJ}/C$ (Q→V integrator), where Q_{FTJ} is the charge involved in the FTJ switching and hereafter interpreted as the FTJ total polarization P. In the integrator setup, R is needed to avoid the OPAMP saturation.

The lumped elements have been designed to allow measurements in the $100\,\mathrm{Hz}$–$10\,\mathrm{kHz}$ frequency range with both circuits. In this respect, the pole frequency f_p defines the circuits bandwidth (BW, inset of Fig. 1) and, as it can be seen, the I→V converter inherently has a low-pass nature, while the Q→V integrator has a high–pass behavior.

In this work, the waveform generator is used to apply a rectangular preset pulse followed by triangular pulses of period $T = f^{-1}$ (Fig. 2, top). Triangular pulses are useful to separate the current peaks due to the ferroelectric switching from the fairly constant current owing to the linear component of the HZO dielectric response (Fig. 2, middle). However, the proposed setup allows the application of any V_T waveform and, for instance, it can be also used for small signal analyses through sinusoidal waves.

4. Experimental results and discussion

Figure 2 shows the typical $I_{FTJ}(t)$ and $Q_{FTJ}(t)$ waveforms measured through the I→V converter (middle) or the Q→V integrator (bottom), respectively. These data are then used to plot the I–V and Q–V curves of the FTJ.
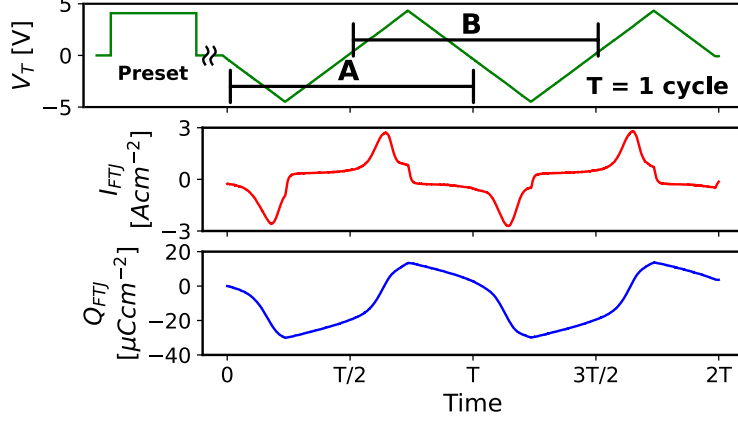
Figure 2: Top: time evolution of the input voltage V_T consisting of a rectangular preset pulse followed by a triangular waveform; Middle: corresponding I_{FTJ} vs. time curves measured through the I→V converter. Flat regions correspond to the FTJ linear dielectric response, while the peaks originate from the ferroelectric switching; Bottom: The Q→V integrator directly measures the evolution during time of the switching charge Q_{FTJ}.

4.1. Optimal measurement condition assessment

Figure 3a shows the I–V and Q–V characteristics recorded during the first triangular pulse period, namely in the $[0; T]$ time interval (Fig. 2, A); the resulting hysteresis loops are open, suggesting a non–optimal measurement. We attribute this behavior to the high depolarization field in the HZO that may cause its back–switching between the end of the preset pulse and the start of the measurement phase [7]. Unfortunately, this time interval is required for the configuration of the instruments and cannot be reduced to zero. Hence, two consecutive triangular pulses are applied to the FTJ and the I–V and Q–V curves are instead extracted from data measured in the $[T/2; 3T/2]$ interval (Fig. 2, B), thus obtaining the closed characteristics of Fig. 3b. Therefore, in the following all results correspond to measurements performed during interval B.

4.2. Equivalence and limitations of proposed circuits

To compare the proposed measuring schemes, the current I_{FTJ} measured through the I→V converter has been numerically integrated in post–processing,
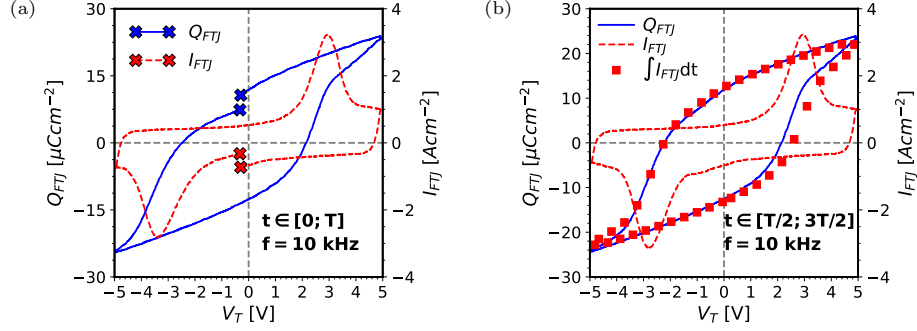
5

Figure 3: Q–V (blue) and I–V (red) curves measured with the setup: (a) curves from the $[0;T]$ interval are open due to the back–switching taking place between the preset and the measurement pulse; (b) curves extracted from the $[T/2;3T/2]$ interval are instead closed. Post–process integration of I_{FTJ} (red squares) is in good agreement with the direct measurement through the Q→V integrator.
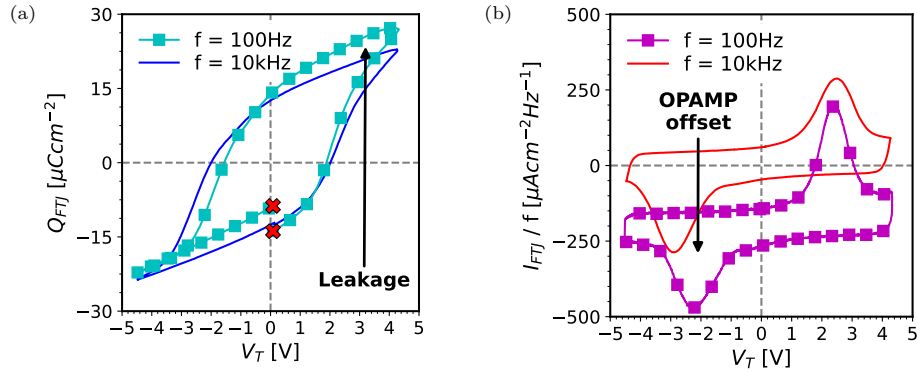

Figure 4: (a) Q–V measured at different frequencies f. At low f, the FTJ static leakage current gets integrated, thus producing a spurious contribution that distorts and opens up the hysteresis loop. (b) I–V curves measured at different f. Since I_{FTJ} is proportional to f, at low frequencies V_{out} may become comparable to the OPAMP output offset, rigidly shifting the I_{FTJ} characteristic. OPAMP offset compensation in post–processing may be possible in this case.
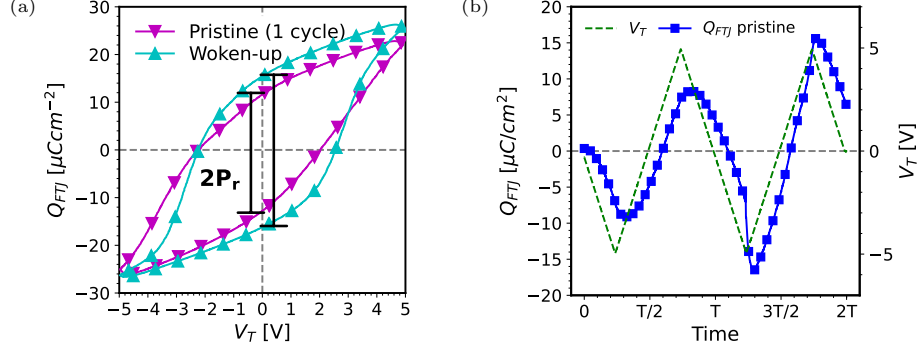
6

Figure 5: (a) Typical enlargement of the hysteresis loop due to the device wake–up, with $2P_r$ increasing from the pristine state (magenta) to the woken–up state (cyan); (b) Q_{FTJ} time evolution in a pristine FTJ.

thus obtaining the Q–V curve depicted in Fig. 3b(red squares), which is in very good agreement with the one obtained from the direct Q_{FTJ} measurement through the Q→V integrator (blue line). This verifies that the measurements through the two circuits are dependable and equivalent.

However, its worth noting that the two amplifiers vastly differ in their BWs (inset of Fig. 1), with the Q→V integrator being more suited for high–frequency measurements. Indeed, the integrator has a lower–limited BW and, furthermore, at low frequencies the integration of undesired current contributions, like the leakage current through the stack, can largely distort the hysteresis loop as shown in Fig. 4a.

On the other hand, the I→V converter can operate down to low frequencies, with the only limitation being the V_{out} amplitude proportional to I_{FTJ} which reduces linearly with a decreasing frequency. So, at very low f the OPAMP output offset may be no longer negligible, thus rigidly shifting the I_{FTJ} characteristic as depicted in Fig. 4b. However, this spurious contribution can be compensated for, hence recovering the correct current characteristics.

4.3. Effects of wake–up and fatigue on FTJ performance

In ferroelectric-based devices, the effects of wake–up and fatigue are widely studied [8]. The FTJ wake–up originates from the redistribution of defects in the ferroelectric layer thanks to the bipolar cycling and it is beneficial for the FTJ performance. In fact, Fig. 5a shows that a not–yet–cycled FTJ (pristine, magenta) has a smaller hysteresis and a lower remnant polarization P_r compared to a woken–up device (cyan). In the latter case, the Q–V exhibits steeper switching branches and increased $2P_r$ window. This effect is also evident in Fig. 5b which reports the time evolution of Q_{FTJ} in a pristine FTJ: the Q_{FTJ} peaks largely increase between the first and second period of the triangular waveform. This clearly confirms that the wake–up sequence is crucial to maximize the FTJ performance and to avoid measurement–to–measurement deviations of the HZO parameters.

However, further cycling has a detrimental effect on the FTJ performance due to the fatigue of the HZO layer. This degradation is clearly visible in Fig. 6a, where different FTJs have been cycled with continuous triangular pulses (5 V amplitude, $f =100\,\mathrm{kHz}$). As it can be seen, $2P_r$ initially increases thanks to the wake–up and then, at approximately 10^3 cycles, it starts to decrease due to the ferroelectric fatigue.

4.4. Preset pulse impact on endurance

The $2P_r$ value has also been monitored after applying different preset pulses before each measurement, observing that the preset tends to induce a higher $2P_r$ with respect to the no–preset case, as summarized in Fig. 6a.

However, Fig. 6a also shows that positive, long presets may induce an early irreversible breakdown of the devices. This has been attributed to the static leakage through the FTJ stack that arises at large positive V_T values [9]. This is evident in the I–V curve in Fig. 6b, which shows a current rise at $V_T=+5\,\mathrm{V}$ after the switching current peak. Conversely, the leakage is not visible for $V_T < 0$, hence negative presets may better preserve the FTJ lifespan, as it is also confirmed by Fig. 6a. This asymmetry in the voltage polarities is due to
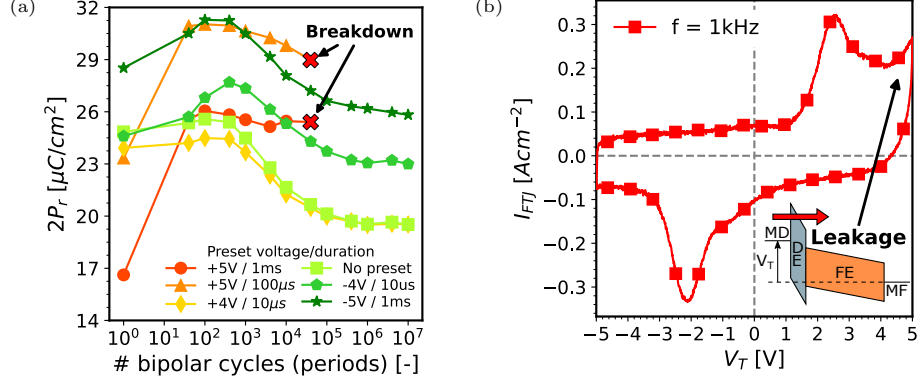
Figure 6: (a) $2P_r$ evolution with cycling (1 cycle = 1 T) for different preset pulses applied before each $2P_r$ measurement. After the initial wake–up, HZO fatigue degrades the device performance. A preset pulse before the measurement is used to improve $2P_r$, but long positive pulses may lead to early breakdown. (b) I–V curve measured applying voltages up to $+5\,$V and down to $-5\,$V. Early breakdown is attributed to the FTJ leakage current, clearly appearing at $+5\,$V due to the conduction band profile depicted in the inset.

the conduction band profile along the device stack, that favors electron injection when V_T is positive (inset of Fig. 6b).

4.5. Frequency–dependent characterization

A large set of FTJs has been characterized for different pulse frequencies and Fig. 7 summarizes the obtained distributions of positive (V_c^+, red) and negative (V_c^-, blue) coercive voltages. V_c^+ and V_c^- have been extracted from the peaks position in the I–V curves. Figure 7 shows that the magnitude of both coercive voltages (especially V_c^-) slightly increases with the measurement frequency, therefore also resulting in an increase of $2V_c = (V_c^+ - V_c^-)$. This is presumably due to the interplay between the ferroelectric switching dynamics described by the Merz's law [10] and the frequency response of the traps at the ferroelectric–dielectric interface [11].
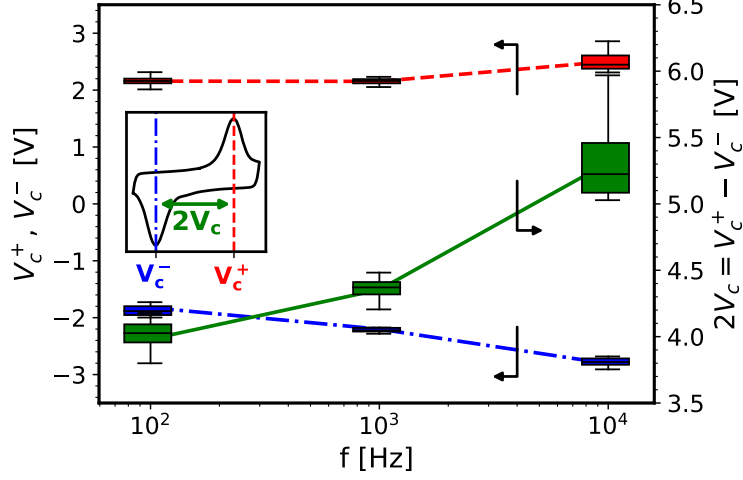
Figure 7: Positive (V_c^+) and negative (V_c^-) coercive voltage distributions of a set of FTJs as a function of the measuring frequency. The magnitude of both slightly increases with f, resulting in an enlarged $2V_c$ window.

5. Conclusions

A low–cost experimental setup was designed to characterize FTJs, allowing the direct measurement of the I–V and Q–V curves through a virtual–grounded I→V converter and Q→V integrator, respectively. The measurement procedure was validated in several respects, thus demonstrating the dependability and versatility of the proposed setup, which can be exploited for a large variety of experiments.

FTJs were investigated as a function of pulse frequency, preset conditions and cycling levels. The applied preset pulses and the HZO wake—up were found to be beneficial for maximizing the $2P_r$ window, and it may also help to reduce measurement–to–measurement and device–to–device variability.

However, it has also been shown that a high number of cycles lead to HZO fatigue and degradation of the FTJ performance. Furthermore, large–positive and long preset pulses may also degrade the ferroelectric material, eventually leading to early breakdown of the devices. This analysis pointed out that, for the FTJs in this work, negative preset pulses are preferable to positive ones in

10

order to enlarge the measured $2P_r$ and still preserve a good FTJ lifespan.

Finally, the measurement frequency slightly influences the extracted coercive voltages that increase with frequency, possibly because of a complex interplay between the HZO dynamics and the interface traps response.

Acknowledgment

References

[1] S. Slesazeck, V. Havel, E. Breyer, H. Mulaosmanovic, M. Hoffmann, B. Max, et al., Uniting the trinity of ferroelectric HfO2 memory devices in a single memory cell, 2019 IEEE 11th Int. Mem. Work. IMW 2019 (may 2019). `doi:10.1109/IMW.2019.8739742`.

[2] S. Yu, Neuro-inspired computing with emerging nonvolatile memories, Proc. IEEE 106 (2) (2018) 260–285. `doi:10.1109/JPROC.2018.2790840`.

[3] S. Slesazeck, T. Mikolajick, Nanoscale resistive switching memory devices: A review, Nanotechnology 30 (35) (2019) 352003. `doi:10.1088/1361-6528/ab2084`.

[4] E. Covi, Q. T. Duong, S. Lancaster, V. Havel, J. Coignus, J. Barbot, et al., Ferroelectric tunneling junctions for edge computing, 2021 IEEE Int. Symp. Circuits Syst. (ISCAS) (2021) 1–5. `doi:10.1109/iscas51556.2021.9401800`.

[5] B. Max, M. Hoffmann, S. Slesazeck, T. Mikolajick, Direct correlation of ferroelectric properties and memory characteristics in ferroelectric tunnel junctions, IEEE J. Electron Devices Soc. 7 (2019) 1175–1181. `doi:10.1109/JEDS.2019.2932138`.

[6] R. Fontanini, M. Segatto, M. Massarotto, R. Specogna, F. Driussi, M. Loghi, D. Esseni, Modeling and design of FTJs as multi-level low energy memristors for neuromorphic computing, IEEE J. Electron Devices Soc. 9 (2021) 1202–1209. `doi:10.1109/JEDS.2021.3120200`.

[7] B. Max, T. Mikolajick, M. Hoffmann, S. Slesazeck, Retention characteristics of Hf0.5Zr0.5O2-based ferroelectric tunnel junctions, 2019 IEEE 11th Int. Mem. Work. IMW 2019 (may 2019). `doi:10.1109/IMW.2019.8739765`.

[8] M. Pešić, F. P. G. Fengler, L. Larcher, A. Padovani, T. Schenk, E. D. Grimley, et al., Physical mechanisms behind the field-cycling behavior of HfO2-based ferroelectric capacitors, Adv. Funct. Mater. 26 (25) (2016) 4601–4612. `doi:10.1002/adfm.201600590`.

[9] J. F. Verweij, J. H. Klootwijk, Dielectric breakdown I: A review of oxide breakdown, Microelectronics J. 27 (7) (1996) 611–622. `doi:10.1016/0026-2692(95)00104-2`.

[10] W. J. Merz, Switching time in ferroelectric BaTiO3 and its dependence on crystal thickness, J. Appl. Phys. 27 (8) (1956) 938–943. `doi:10.1063/1.1722518`.

[11] V. Mikheev, A. Chouprik, Y. Lebedinskii, S. Zarubin, Y. Matveyev, E. Kondratyuk, et al., Ferroelectric second-order memristor, ACS Appl. Mater. Interfaces 11 (35) (2019) 32108–32114. `doi:10.1021/acsami.9b08189`.